Impact of Short-Wavelength and Long-Wavelength Line-Edge Roughness on the Variability of Ultrascaled FinFETs

Michael Wong, Kyle D. Holland, *Member, IEEE*, Sam Anderson, Shahriar Rizwan, Zhi Cheng (Jason) Yuan, Terence B. Hook, Diego Kienle, Prasad S. Gudem, *Senior Member, IEEE*, and Mani Vaidyanathan, *Member, IEEE*

***Abstract*— We examine the impact of line-edge roughness (LER) on the variability in the on-current and saturation threshold voltage of ultrascaled FinFET devices via quantum-mechanical transport simulation. We obtain a realistic model of LER by decomposing the LER into short-λ and long-λ fluctuations, and we consider their separate influences on device performance. We show that the long-λ fluctuations lead to greater device variability than the short-λ fluctuations, and we explain the difference between the two cases via the influence of fluctuating quantum confinement arising from the LER. Finally, we consider devices in which the long-λ fluctuations of the two fin edges are correlated and demonstrate that this correlation significantly improves the variability. Thus, we show the continued need for fabrication technology either to reduce the amplitude of the long-λ fluctuations or to ensure the long-λ fluctuations between the sidewalls of ultrascaled FinFET devices are correlated.**

***Index Terms*— FinFET, line-edge roughness (LER), nonequilibrium Green's function, surface roughness, variability.**

I. Introduction

As FinFET devices scale toward ever-smaller dimensions, line edge roughness (LER) becomes an increasingly important contributor to device variability [1]. Developing manufacturing processes for advanced FinFET technologies will therefore require a thorough understanding of the physical mechanisms responsible for translating LER fluctuations to device variance.

There have been many studies investigating the impact of LER on the variability of FinFETs, in which LER profiles are randomly generated, and ensembles of FinFET devices are simulated in order to determine the resulting variability [1]–[13]. Furthermore, some studies have also considered the effect of correlated LER [1]–[5], concluding that correlation significantly improves variability. When generating the LER profiles, these studies typically start from an assumed Gaussian [14] or exponential [15] autocovariance function and reconstruct the spatial profile with random phase injection.

Early interface characterization studies [14], [15] consider profile variation at spatial frequencies that are on the order of the atomic spacing with $\lambda \sim 1$ nm (henceforth termed "short-λ fluctuation"), but fluctuations at a much larger length scale ($\lambda \geq 10$ nm, henceforth termed "long-λ fluctuation") have also been demonstrated [16]. Moreover, fluctuation at these two length scales has been shown to coexist. For example, Goodnick *et al.* [15] noted "very-long-wavelength fluctuations in the surface which are uncorrelated with the shorter range fluctuations," but did not consider them in their characterization. Other characterization studies have also identified fluctuations at both short-λ and long-λ length scales [17], [18].

While studies have been conducted that examine the influence of either short-λ or long-λ fluctuation, there has been no study yet, to the best of our knowledge, that considers both and compares their impact on device behavior. In this paper, we perform quantum-mechanical transport simulations of multiple ensembles of ultrascaled FinFET devices with various classes of LER profiles. We separately investigate short-λ, long-λ, and correlated long-λ fluctuations, as well as relevant combinations, and explain the differences among the resulting distributions in ON-current (I_{ON}) and saturation threshold voltage (V_{th}) by considering the influence of fluctuating quantum confinement. We show that, when fabricating ultrascaled FinFETs, long-λ fluctuations tend to be more detrimental to device variability. Therefore, it is important to mitigate the long-λ fluctuations in ultrascaled FinFET technology, or to use a process that ensures correlation between the two sidewalls.

II. Device Description

A. Nominal Device

We consider a device with channel length $L_g = 8$ nm and nominal fin width $W_{fin} = 4$ nm as a representative ultrascaled FinFET, as shown in Fig. 1. The channel material is silicon,

Manuscript received December 1, 2016; accepted January 4, 2017. Date of publication February 13, 2017; date of current version February 24, 2017. This work was supported in part by the Natural Sciences and Engineering Research Council of Canada, and in part by Alberta Innovates Technology Futures. The review of this paper was arranged by Editor M. S. Bakir.

M. Wong, K. D. Holland, S. Anderson, S. Rizwan, Z. C. Yuan, and M. Vaidyanathan are with the Department of Electrical and Computer Engineering, University of Alberta, Edmonton, AB T6G 2V4, Canada (e-mail: maniv@ualberta.ca).

T. B. Hook is with IBM Corporation, Essex Junction, VT 05452 USA.

D. Kienle is with the Theoretische Physik I, Universität Bayreuth, 95440 Bayreuth, Germany.

P. S. Gudem is with Qualcomm Technologies Inc., San Diego, CA 92121 USA.

Color versions of one or more of the figures in this paper are available online at http://ieeexplore.ieee.org.

Digital Object Identifier 10.1109/TED.2017.2655520

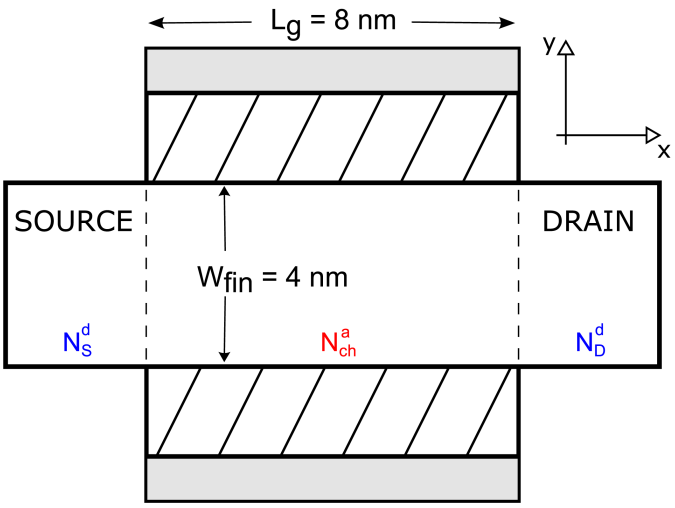

Fig. 1. Top–down view of the nominal FinFET device in this paper. Transport occurs in the *x*-direction and confinement occurs in the *y*-direction. Physical parameters for this device are summarized in Table I.

TABLE I
PHYSICAL DEVICE PARAMETERS

Gate Length	L_g	8 nm
Channel Length	L_{ch}	8 nm
Fin Width	W_{fin}	4 nm
Oxide Thickness	t_{ox}	2 nm
Oxide Dielectric Constant	$\varepsilon_{r,\text{ox}}$	12.5
Gate Workfunction	Φ_{g}	4.52 eV
Source/Drain Doping (n-type)	$N^d_{\text{S/D}}$	2×10^{20} cm^{-3}
Channel Doping (p-type)	N^a_{ch}	1×10^{17} cm^{-3}

with transport aligned in the (100) direction. The doping follows a step profile, with a background p-type doping of $N^a_{\text{ch}} = 1\times10^{17}$ cm^{-3} in the channel, and a source/drain n-type doping of $N^d_{S/D} = 2\times10^{20}$ cm^{-3}. The physical parameters of the nominal device are summarized in Table I. Fin height is omitted due to the 2-D nature of the simulations performed, as further explained in Section III.

B. Generation of LER Profiles

Rough devices are generated by superimposing short- and long-λ fluctuations $A_S(x)$ and $A_L(x)$ on the sidewalls of the nominal device.

Short-λ fluctuations are generated using an exponential autocovariance as outlined in [15]

$$C(x) = \Delta_m^2 e^{-(\sqrt{2}x/L_m)} \xrightarrow{\substack{\textit{reconstruct with}\\ \textit{random phase}}} A_S(x) \qquad (1)$$

where Δ_m is the root-mean-square value of the roughness profile, and L_m is the correlation length. In this paper, we use roughness parameters $\Delta_m = 1.5$ Å and $L_m = 8.75$ Å, which align well with the experimental findings given in [15, Table I].

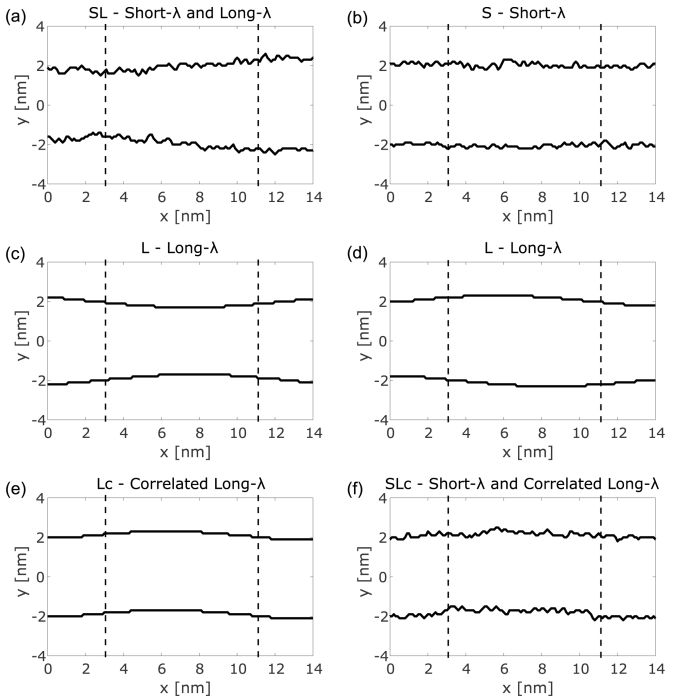

Fig. 2. Various classes of LER profiles considered in this paper, as summarized in Table II. Dashed lines denote the start and end of the channel region. (a) SL-class device, depicting short-λ fluctuation superimposed on long-λ fluctuation. (b) S-class device. (c) L-class device, depicting long-λ fluctuations resulting in a narrower channel. (d) L-class device, depicting long-λ fluctuations resulting in a wider channel. (e) Lc-class device. (f) SLc-class device, depicting short-λ fluctuation superimposed on correlated long-λ fluctuation.

Long-λ fluctuations are represented by a simple sine wave

$$A_L(x) = A_m \sin\left(\frac{2\pi x}{\lambda_m} + \phi_m\right) \qquad (2)$$

where A_m is the amplitude of the fluctuation, λ_m is the wavelength, and ϕ_m is the phase offset, which is taken to be uniformly distributed. We take $\lambda_m = 20$ nm because setting $\lambda_m > L_{\text{ch}}$ allows the long-λ fluctuation to account for various channel shapes. For example, it is possible to obtain both a channel that is narrower in the middle, and a channel that is wider in the middle, as shown in Fig. 2(c) and (d), respectively. In order to choose a value for A_m, we observe that the chosen short-λ parameters tend to yield peak deviations of ~3 Å from the nominal value. Therefore, we set $A_m = 3$ Å for the sake of making a fair comparison. Correlated long-λ fluctuations can be obtained by using the same ϕ_m value in (2) for both sidewalls.

C. Rough Devices

In this paper, we examine five different classes of LER profiles, summarized in Table II, with examples in Fig. 2. First, devices with both types of fluctuation are considered (SL-class devices), the profiles of which are obtained by superimposing generated short-λ fluctuations on a long-λ profile. Then, we investigate the effect of each roughness type separately (S-class and L-class devices). Finally, we force the long-λ to be perfectly correlated between the two sidewalls,

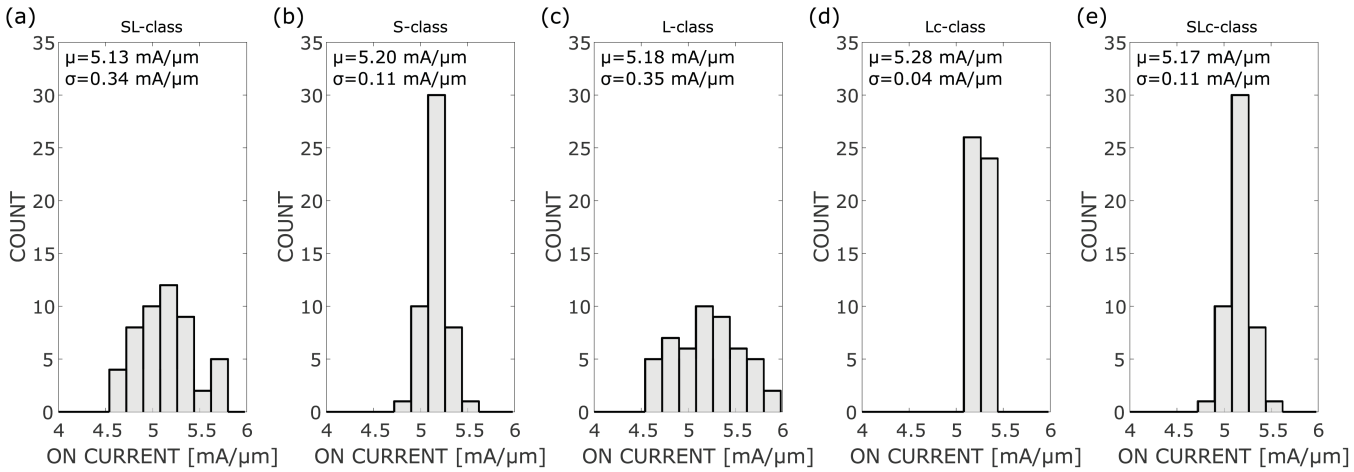

Fig. 3. Distributions of I_{ON}, characterized by mean μ and standard deviation σ, for the five LER profile classes considered in this paper. Note that profiles with uncorrelated long-λ components exhibit a significantly higher spread. Mean I_{ON} values for each distribution should be compared with the value $I_{ON,sm} = 5.41$ mA/μm for a smooth device. (a) SL-class. (b) S-class. (c) L-class. (d) Lc-class. (e) SLc-class.

both with (SLc-class devices) and without (Lc-class devices) the short-λ fluctuations.

III. Simulation Methodology

In order to determine the characteristics of a given FinFET, we employ an in-house device solver [19], [20] that uses the nonequilibrium Green's function formalism [21] to solve the quantum transport problem self-consistently with the Poisson equation. Such an approach is well-equipped to study the physics underlying device operation, as the influence of quantum effects, such as confinement and tunneling, is inherently captured by the formalism. We consider transport through the six conduction band valleys of silicon with $m_l^* = 0.91m_e$ and $m_t^* = 0.19m_e$, where m_l^* and m_t^* denote the longitudinal and transverse effective masses, respectively [22], [23]. Since we are interested in isolating the impact of LER, other device nonidealities, such as Coulombic scattering or phonon scattering, are omitted in this paper. The omission of phonon scattering is further justified by the short channel length of our devices relative to the electron mean-free path due to phonon scattering in silicon ($l_{mfp,phon} \sim 40$ nm) [24], [25].

As a result of the strong quantum confinement present in FinFET devices, only a few subbands, or modes, are relevant to transport. Therefore, we employ a coupled mode-space approach [26], exploiting the low number of subbands for efficient solution of the transport problem. Once the mode-space Hamiltonian is constructed, contact self-energies are computed using the Sancho–Rubio iterative method [27].

In order to keep the computational workload feasible, we perform 2-D simulations for each device. We assume translational invariance in the fin height direction, and incorporate its effect into our solution via the use of integrated Fermi–Dirac integrals [21], an approach that is justified by recent trends in industry of high aspect ratio fins [28], [29] ($H_{fin} \sim 25$–35 nm for $W_{fin} = 4$ nm).

The assumption of translational invariance neglects several phenomena, such as confinement effects due to finite fin height, as well carrier scattering off the top and bottom of the fin. However, these effects can be considered to be of secondary importance, because the fins are sufficiently tall. Another phenomenon not captured in our simulations is the influence of any roughness along the fin sidewall in the fin height direction, which will result in an underestimation of the full impact of fin sidewall roughness on device performance. Nonetheless, within the context of a comparison between types of LER, these 2-D simulations can still reveal useful, *qualitative* insights regarding the impact of LER on device performance.

TABLE II
Classes of LER Profiles

Class Label	Description
SL	Short-λ + Long-λ
S	Short-λ
L	Long-λ
Lc	Correlated Long-λ
SLc	Short-λ + Correlated Long-λ

IV. Results and Discussion

A. Influence of Short-λ and Long-λ Fluctuations

For the purposes of comparison, we simulated a smooth device with no LER as a reference, obtaining $I_{ON,sm} = 5.41$ mA/μm, where I_{ON} is defined as the current at $V_{GS} = V_{DS} = 0.75$ V. We then considered the variability arising from the various LER profiles classified in Table II, found by simulating a number of devices for each profile type. The results are summarized in Fig. 3 in the format of histograms, showing the distribution of ON-current values, characterized by mean μ and standard deviation σ.

We first consider the variability of SL-class devices, characterized by both short-λ and long-λ fluctuations, for which the results are shown in Fig. 3(a). The mean I_{ON} drops to 5.13 mA/μm from $I_{ON,sm} = 5.41$ mA/μm. Moreover, we observe that SL-class devices exhibit a relatively large spread, with a standard deviation of $\sigma = 0.34$ mA/μm.

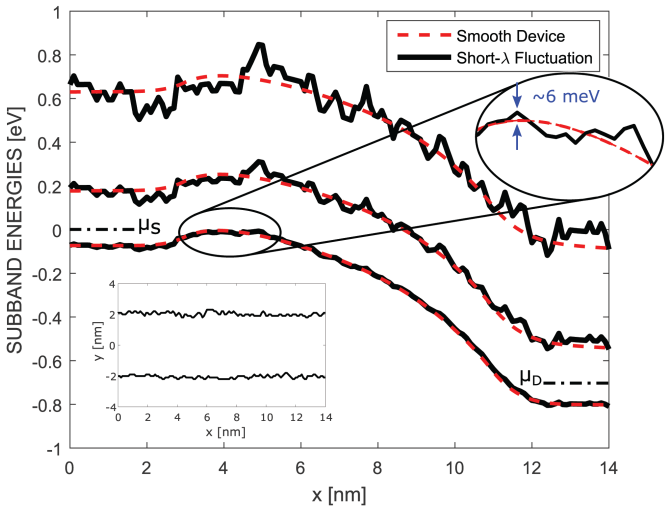

Fig. 4. Profiles for the first three subbands of an S-class device with short-λ fluctuation for Si valley $m_x^* = 0.91m_e$, $m_y^* = 0.19m_e$, and $m_z^* = 0.19m_e$. For this device, $I_{ON} = 4.95$ mA/μm. Profiles for a smooth device are also shown (dashed lines) for comparison. The corresponding LER pattern is shown in the inset.

To investigate the cause of this significant variability, we consider the influence of each type of fluctuation separately. Fig. 3(b) and (c) clearly show that L-class devices exhibit a much larger spread ($\sigma = 0.35$ mA/μm) than S-class devices ($\sigma = 0.11$ mA/μm), suggesting that the long-λ fluctuations are largely responsible for the variability in SL-class devices. It is also noteworthy that, whenever long-λ fluctuations are present (with or without short-λ fluctuations), there is a significant chance that a device could have I_{ON} greater than $I_{ON,sm}$, as shown by the significant occurrence of high ON-current values in the histograms of Fig. 3(a) and (c). On the other hand, the presence of short-λ fluctuations alone is unlikely to cause a larger I_{ON} than the smooth device, as shown by the histogram of Fig. 3(b). These trends in μ and σ can be explained by considering the various internal physical quantities provided by our simulation, as follows.

We examine the subband profile plots for various device classes. These plots are constructed from the eigenenergies that emerge from the solution of the Schrödinger equation

$$\left[-\frac{\hbar^2}{2m_y^*}\frac{\partial^2}{\partial y^2} - qV(x_i, y)\right]\psi_j(x_i, y) = \varepsilon_j(x_i)\psi_j(x_i, y) \quad (3)$$

which is solved for each transport valley within our mode-space approach and at each value x_i along the channel. After solving at each position x_i in the transport direction, we can plot the eigenenergies $\varepsilon_j(x)$ versus x, which yields the band profile for electrons in the corresponding conduction subband. All such plots in this paper show the subband profiles for the valley with $m_x^* = 0.91m_e$, $m_y^* = 0.19m_e$, and $m_z^* = 0.19m_e$, but the corresponding discussion applies to the other valleys, as similar features were observed in all three sets.

Shown in Fig. 4 are the subband profiles for an S-class device with $I_{ON} = 4.95$ mA/μm, as well as for the smooth device. The presence of short-λ fluctuation produces a jaggedness in the subband profiles, with variations occurring at length scales on the order of 1 nm. This jaggedness is a direct result of varying confinement arising from the rapid changes in W_{fin} due to short-λ LER. Each cross-sectional slice can be viewed as a finite square well of width W_{fin}, and it is well-known that changing the width of a square well results in a change in the eigenenergies [30]. While higher eigenenergies will be more affected [30], visible in the increased jaggedness at the higher subbands, jaggedness is also present in the lower subbands, as illustrated by the zoomed-in view in Fig. 4. These lower subbands are the most relevant to carrier transport, since they are closest to the source Fermi level and hence see the highest number of electrons injected by the source; the extreme fin width confinement results in a subband separation large enough for the higher modes to be well removed from the source Fermi level. For example, for the valley shown in Fig. 4, only the first two modes play a role in transport.

The peaks in the subband profiles of Fig. 4 resulting from the jaggedness lead to barriers to electron flow, and hence, a degradation in I_{ON} in comparison with the case of a smooth fin. However, because the short-λ fluctuations occur at a high spatial frequency (recall $L_m = 8.75$ Å), any given constriction in the fin width that occurs due to short-λ fluctuations is unlikely to persist for greater than 1 nm of the channel length. Thus, the peaks in the profiles tend to act as barriers that are less than 1 nm thick, through which electrons can pass via quantum tunneling. In other words, these subnanometer-scale features of the subband profiles are less significant than the *general shape* of the profiles, which remains similar between the smooth and rough devices, as shown in Fig. 4. This explains the lower degree of variability in S-class devices.

On the other hand, the subband profiles for L-class devices look drastically different from those of the smooth device. Fig. 5(a) shows the subband profiles for an L-class device in which the LER causes a narrower channel than nominal. This device has a notably degraded ON-current $I_{ON} = 4.58$ mA/μm, as the narrower W_{fin} in the gated region (3 nm $\leq x \leq$ 11 nm) results in a significantly increased source–drain barrier height for all the subbands, arising from increased confinement in the gated region. In contrast, Fig. 5(b) shows the subband profiles for an L-class device in which the LER causes a wider channel than nominal. Here, $I_{ON} = 5.89$ mA/μm, which is actually greater than the ON-current of the nominal device, as the wider W_{fin} in the channel region results in reduced source–drain barriers, and therefore increased transmission of carriers from source to drain. As with Fig. 4, the zoomed-in views in Fig. 5(a) and (b) show that the barrier heights are indeed affected in the lowest modes, even though more visible in the higher modes; the deviations of several millielectronvolts in comparison with the smooth device are sufficient to impact the device characteristics.

B. Correlated Long-λ Fluctuations

In order to gain more insight into the influence of long-λ fluctuations on device performance, we also consider devices wherein the long-λ LER components of each sidewall are correlated. Note that such correlation is potentially achievable by present-day fabrication techniques. For exam-

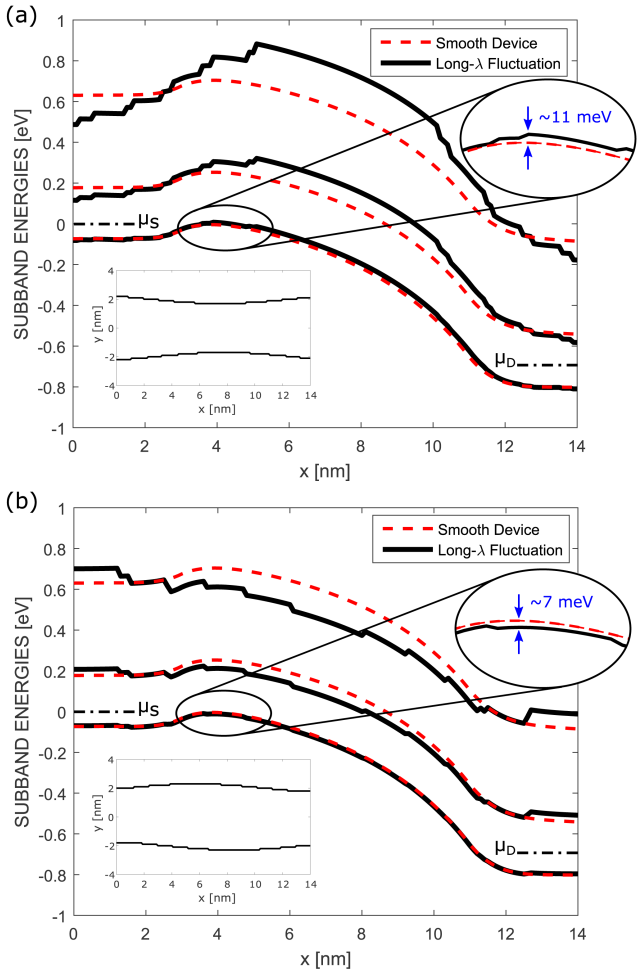

Fig. 5. Profiles for the first three subbands of L-class devices with long-λ fluctuation. Profiles for a smooth device are also shown (dashed lines) for comparison. The corresponding LER patterns are shown in the insets. (a) Device with the narrower channel exhibits higher barriers to electron flow than the smooth device and has $I_{ON} = 4.58$ mA/μm. (b) Device with wider channel exhibits lower barriers to electron flow than the smooth device and has $I_{ON} = 5.89$ mA/μm.

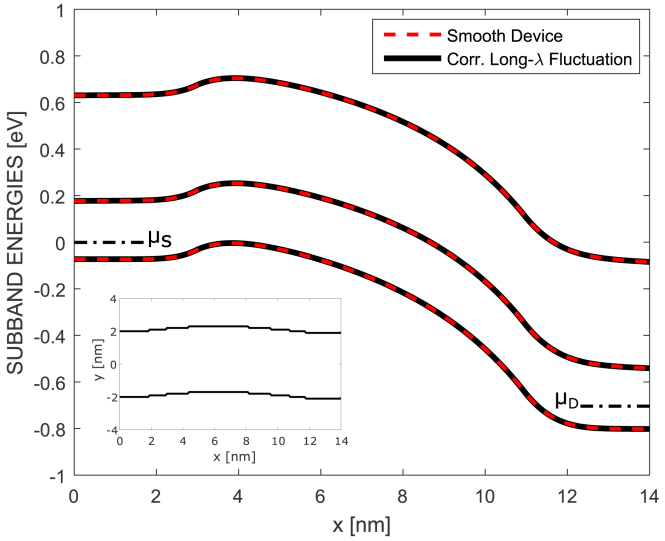

Fig. 6. Profiles for the first three subbands of an Lc-class device with correlated long-λ fluctuation. For this device, $I_{ON} = 5.25$ mA/μm. Profiles for a smooth device are also shown (dashed lines), but overlap with the Lc-class device profiles due to constant fin width. The corresponding LER profile is shown in the inset.

ple, spacer lithography can result in a strong correlation between fin sidewalls at the long-λ length scale [31]. On the other hand, we do not consider correlation at the short-λ length scale, because currently there exists no mechanism for fabrication technology to enforce correlation at the atomic scale.

By comparing the results in Fig. 3 for SL-class devices ($\sigma = 0.34$ mA/μm) to SLc-class devices ($\sigma = 0.11$ mA/μm), we see that correlation at the long-λ scale leads to a noticeable improvement in variability. This trend is further reinforced by the comparison between L-class devices ($\sigma = 0.35$ mA/μm) and Lc-class devices ($\sigma = 0.04$ mA/μm). The reason for this improved variability can be clearly seen in Fig. 6. A device with perfectly correlated LER exhibits a uniform fin width, and therefore, the eigenvalue spread does not vary significantly between positions x_i. Thus, the subband profiles are nearly identical to the subband profiles of a smooth device. This holds true for all Lc-class devices, resulting in very little variability in I_{ON}.

It is also interesting to note that, despite the nearly identical subband profiles across all Lc-class devices, the average I_{ON} still drops slightly to 5.29 mA/μm, and variability is still present. Both of these observations can be attributed to a degradation mechanism known as wave function deformation scattering. This effect, which cannot be inferred by examining the shapes of the subband profiles, is due to the changing shape of the wave function [$\psi_j(x_i, y)$ in (3)] between adjacent positions x_i, which results in a lowered transmission from source to drain [32].

C. Threshold Voltage Variability

We also present saturation threshold voltage (V_{th}) values, where V_{th} is defined via the constant-current method as the gate voltage needed to obtain a current of 37.5 μA/μm when $V_{DS} = 0.75$ V. For the smooth device, $V_{th,sm} = 177.9$ mV. As shown in Fig. 7, V_{th} variability follows the same trends observed in I_{ON} variability. Namely, long-λ fluctuations [Fig. 7(c), $\sigma = 7.4$ mV] result in significantly greater variability in V_t than short-λ fluctuations [Fig. 7(b), $\sigma = 1.7$ mV]. Furthermore, by comparing L-class devices ($\sigma = 7.4$ mV) to Lc-class devices ($\sigma = 0.3$ mV) and SL-class devices ($\sigma = 7.2$ mV) to SLc-class devices ($\sigma = 1.9$ mV), we see that enforcing correlation in the long-λ fluctuations again greatly reduces the variability in V_{th}.

These observations can also be explained by considering the subband profiles of the various devices. Since the subband profiles of an S-class device have the same general shape as the smooth device, but with a superimposed jaggedness, a similar gate voltage is required to modulate the barriers enough to achieve the target current across all S-class devices. Variability does arise due to the stochastic nature of the jaggedness, but as explained earlier, this jaggedness has a reduced impact on the resulting current due to quantum tunneling effects. The

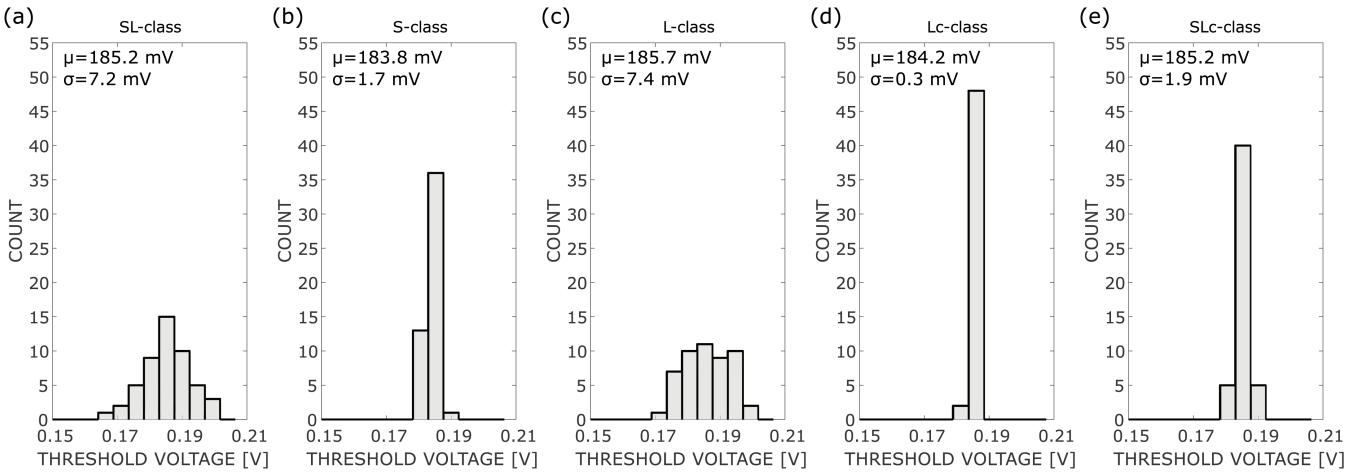

Fig. 7. Distributions of V_{th}, characterized by mean μ and standard deviation σ, for the five LER profile classes considered in this paper. As with I_{ON}, the profiles with uncorrelated long-λ components exhibit a significantly higher spread. Mean V_{th} values for each distribution should be compared with the value $V_{th,sm} = 177.9$ mV for a smooth device. (a) SL-class. (b) S-class. (c) L-class. (d) Lc-class. (e) SLc-class.

subband profiles of an L-class device, on the other hand, exhibit significantly changed barriers to electron flow, and therefore, we see that a relatively large spread of gate voltages is required to reach the target current.

V. Conclusion

The following conclusions can be drawn from this paper on the impact of LER on FinFET variability.

1) LER can occur in the form of fluctuations at short-λ and long-λ length scales, and both types of fluctuation can occur simultaneously. Each type arises from different physical processes, and impacts device characteristics in different ways.
2) One mechanism by which LER affects device performance is the formation of fluctuations in the fin width, leading to fluctuations in quantum confinement and hence fluctuations in the subband profiles.
3) Long-λ fluctuations cause greater device variability than short-λ fluctuations, because long-λ fluctuations can cause significant changes in the overall shape of the subband profiles, whereas short-λ fluctuations induce jaggedness on a small length scale.
4) Enforcing correlation between the fin sidewalls at the long-λ length scale effectively removes the variations in the subband profiles, significantly reducing variability.

We also note here that, in advanced FinFETs, other sources of nonidealities, such as random dopant fluctuation or work function variation, may have an equal or greater impact on variability than LER [33]. However, given that LER is one potentially significant source of variability, this paper shows that it is important to consider whether short-λ or long-λ LER fluctuations are reduced when considering fabrication methods to mitigate roughness in ultrascaled FinFETs (e.g., spacer lithography [31], sacrificial oxidation [34], or H_2 annealing [35]).

Furthermore, our demonstration of the improved variability with correlated sidewalls reemphasizes the importance of correlation in controlling device variability. Spacer lithography, which results in strong correlation at long-λ length scales, has become the industry standard for fabrication of FinFET technology at present-day technology nodes; however, this method is used mainly due to its ability to achieve sublithographic fin pitch [31], while the sidewall correlation is just an additional benefit. As industry looks toward scaling fin size and pitch even more aggressively, more exotic approaches that do not necessarily lead to naturally correlated fin sidewalls, such as directed self-assembly of block copolymers [36]–[38], have garnered interest. When evaluating such methods, it is important to consider not only the minimum achievable fin pitch, but also the nature of the long-λ fluctuations in the fin sidewalls. In order to minimize potential impacts of LER, a manufacturing technology must produce fins with long-λ LER fluctuations that are either low in amplitude, or strongly correlated between the fin sidewalls.

Acknowledgment

The authors would like to thank International Business Machines Corporation for the valuable discussions held throughout the course of this paper.

References

[1] E. Baravelli, A. Dixit, R. Rooyackers, M. Jurczak, N. Speciale, and K. D. Meyer, "Impact of line-edge roughness on FinFET matching performance," *IEEE Trans. Electron Devices*, vol. 54, no. 9, pp. 2466–2474, Sep. 2007.

[2] A. Dixit *et al.*, "Impact of stochastic mismatch on measured SRAM performance of FinFETs with resist/spacer-defined fins: Role of line-edge-roughness," in *Proc. IEEE Int. Electron Devices Meeting*, San Francisco, CA, USA, Dec. 2006, pp. 1–4.

[3] X. Jiang, R. Wang, T. Yu, J. Chen, and R. Huang, "Investigations on line-edge roughness (LER) and line-width roughness (LWR) in nanoscale CMOS technology: Part I–modeling and simulation method," *IEEE Trans. Electron Devices*, vol. 60, no. 11, pp. 3669–3675, Nov. 2013.

[4] R. Wang *et al.*, "Investigations on line-edge roughness (LER) and line-width roughness (LWR) in nanoscale CMOS technology: Part II–experimental results and impacts on device variability," *IEEE Trans. Electron Devices*, vol. 60, no. 11, pp. 3676–3682, Nov. 2013.

[5] C.-Y. Chen, W.-T. Huang, and Y. Li, "Electrical characteristic and power consumption fluctuations of trapezoidal bulk FinFET devices and circuits induced by random line edge roughness," in *Proc. 16th Int. Symp. Quality Electron. Design*, Santa Clara, CA, USA, Mar. 2015, pp. 61–64.

[6] S. Yu *et al.*, "3-D simulation of geometrical variations impact on nanoscale FinFETs," in *Proc. 9th Int. Conf. Solid-State Integr.-Circuit Technol.*, Beijing, China, Oct. 2008, pp. 408–411.
[7] Y.-S. Wu, M.-L. Fan, and P. Su, "Impact of surface orientation on Vth variability of FinFET," in *Proc. Silicon Nanoelectronics Workshop*, Honolulu, HI, USA, Jun. 2010, pp. 1–2.
[8] G. Leung and C. O. Chui, "Variability in inversion-mode and junctionless FinFETs due to line edge roughness," *IEEE Electron Device Lett.*, vol. 32, no. 11, pp. 1489–1491, Nov. 2011.
[9] G. Indalecio, A. García-Loureiro, M. Aldegunde, and K. Kalna, "Study of statistical variability in nanoscale transistors introduced by LER, RDF and MGG," in *Proc. Spanish Conf. Electron Devices*, Valladolid, Spain, Feb. 2013, pp. 95–98.
[10] C.-J. Chen, Y.-N. Chen, M.-L. Fan, V. P.-H. Hu, P. Su, and C.-T. Chuang, "Impacts of work function variation and line-edge roughness on TFET and FinFET devices and logic circuits," in *Proc. IEEE SOI-3D-Subthreshold Microelectron. Technol. Unified Conf.*, Millbrae, CA, USA, Oct. 2014, pp. 1–2.
[11] Y. Xiao, B. Zhang, H. Lou, X. Cui, X. Lin, and L. Zhang, "Impact of channel line-edge roughness on junctionless FinFET," in *Proc. IEEE Int. Conf. Electron Devices Solid-State Circuits*, Singapore, Jun. 2015, pp. 106–109.
[12] N. Seoane *et al.*, "Comparison of fin-edge roughness and metal grain work function variability in InGaAs and Si FinFETs," *IEEE Trans. Electron Devices*, vol. 63, no. 3, pp. 1209–1216, Mar. 2016.
[13] A. Martinez, N. Seoane, A. R. Brown, J. R. Barker, and A. Asenov, "Variability in Si nanowire MOSFETs due to the combined effect of interface roughness and random dopants: A fully three-dimensional NEGF simulation study," *IEEE Trans. Electron Devices*, vol. 57, no. 7, pp. 1626–1635, Jul. 2010.
[14] R. E. Prange and T.-W. Nee, "Quantum spectroscopy of the low-field oscillations in the surface impedance," *Phys. Rev.*, vol. 168, no. 3, pp. 779–786, 1968.
[15] S. M. Goodnick, D. K. Ferry, C. W. Wilmsen, Z. Liliental, D. Fathy, and O. L. Krivanek, "Surface roughness at the Si(100)-SiO_2 interface," *Phys. Rev. B*, vol. 32, no. 12, pp. 8171–8186, Dec. 1985.
[16] A. Asenov, S. Kaya, and A. R. Brown, "Intrinsic parameter fluctuations in decananometer MOSFETs introduced by gate line edge roughness," *IEEE Trans. Electron Devices*, vol. 50, no. 5, pp. 1254–1260, May 2003.
[17] O. Krivanek and J. Mazur, "The structure of ultrathin oxide on silicon," *Appl. Phys. Lett.*, vol. 37, no. 4, pp. 392–394, Aug. 1980.
[18] X. Tang *et al.*, "A simple method for measuring Si-fin sidewall roughness by AFM," *IEEE Trans. Nanotechnol.*, vol. 8, no. 5, pp. 611–616, Sep. 2009.
[19] K. D. Holland, N. Paydavosi, N. Neophytou, D. Kienle, and M. Vaidyanathan, "RF performance limits and operating physics arising from the lack of a bandgap in graphene transistors," *IEEE Trans. Nanotechnol.*, vol. 12, no. 4, pp. 566–577, Jul. 2013.
[20] K. D. Holland *et al.*, "Impact of contact resistance on the f_T and f_{max} of graphene versus MoS_2 transistors," *IEEE Trans. Nanotechnol.*, vol. 16, no. 1, pp. 94–106, Jan. 2017.
[21] S. Datta, "Nanoscale device modeling: The Green's function method," *Superlattices Microstruct.*, vol. 28, no. 4, pp. 253–278, Oct. 2000.
[22] J. C. Hensel, H. Hasegawa, and M. Nakayama, "Cyclotron resonance in uniaxially stressed silicon. II. Nature of the covalent bond," *Phys. Rev.*, vol. 138, no. 1A, pp. A225–A238, Apr. 1965.
[23] A. Rahman, M. Lundstrom, and A. W. Ghosh, "Generalized effective-mass approach for n-type metal-oxide-semiconductor field-effect transistors on arbitrarily oriented wafers," *J. Appl. Phys.*, vol. 97, no. 5, pp. 053702-1–053702-12, Mar. 2005.
[24] L. Weber and E. Gmelin, "Transport properties of silicon," *Appl. Phys. A, Solids Surf.*, vol. 53, no. 2, pp. 136–140, Aug. 1991.
[25] K. H. Cho *et al.*, "Experimental evidence of ballistic transport in cylindrical gate-all-around twin silicon nanowire metal-oxide-semiconductor field-effect transistors," *Appl. Phys. Lett.*, vol. 92, no. 5, pp. 052102-1–052102-3, Feb. 2008.
[26] R. Venugopal, Z. Ren, S. Datta, M. S. Lundstrom, and D. Jovanovic, "Simulating quantum transport in nanoscale transistors: Real versus mode-space approaches," *J. Appl. Phys.*, vol. 92, no. 7, pp. 3730–3739, Oct. 2002.
[27] M. P. L. Sancho, J. M. L. Sancho, and J. Rubio, "Highly convergent schemes for the calculation of bulk and surface Green functions," *J. Phys. F, Met. Phys.*, vol. 15, no. 4, pp. 851–858, Apr. 1985.
[28] M. Bardon *et al.*, "Dimensioning for power and performance under 10nm: The limits of FinFETs scaling," in *Proc. Int. Conf. IC Design Technol.*, Leuven, Belgium, 2015, pp. 1–4.
[29] S. Natarajan *et al.*, "A 14nm logic technology featuring 2^{nd}-generation FinFET, air-gapped interconnects, self-aligned double patterning and a 0.0588 μm^2 SRAM cell size," in *IEEE Int. Electron Devices Meeting*, San Francisco, CA, USA, Dec. 2014, pp. 3.7.1–3.7.3.
[30] B. H. Bransden and C. J. Joachain, "One-dimensional examples," in *Quantum Mechanics*, vol. 4., 2nd ed. New York, NY, USA: Pearson, pp. 133–192, 2000.
[31] Y. K. Choi *et al.*, "Sub-20 nm CMOS FinFET technologies," *IEEE Int. Electron Devices Meeting Tech. Dig.*, Washington, DC, USA, Dec. 2001, pp. 19.1.1–19.1.4.
[32] J. Wang, E. Polizzi, A. Ghosh, S. Datta, and M. Lundstrom, "A quantum mechanical approach for the simulation of Si/SiO2 interface roughness scattering in silicon nanowire transistors," *J. Comput. Electron.*, vol. 3, nos. 3–4, pp. 453–457, Oct. 2004.
[33] S. Agarwal, T. B. Hook, M. Bajaj, K. McStay, W. Wang, and Y. Zhang, "Transistor matching and fin angle variation in FinFET technology," *IEEE Trans. Electron Devices*, vol. 62, no. 4, pp. 1357–1359, Apr. 2015.
[34] W. H. Juan and S. W. Pang, "Controlling sidewall smoothness for micromachined Si mirrors and lenses," *J. Vac. Sci. Technol. B*, vol. 14, no. 6, pp. 4080–4084, Nov./Dec. 1996.
[35] M.-C. M. Lee and M. C. Wu, "Thermal annealing in hydrogen for 3-D profile transformation on silicon-on-insulator and sidewall roughness reduction," *J. Microelectromech. Syst.*, vol. 15, no. 2, pp. 338–343, Apr. 2006.
[36] I. W. Hamley, "Nanotechnology with soft materials," *Angew. Chem. Int. Ed.*, vol. 42, no. 15, pp. 1692–1712, Apr. 2003.
[37] D. P. Sanders *et al.*, "Integration of directed self-assembly with 193nm lithography," *J. Photopolymer Sci. Technol.*, vol. 23, no. 1, pp. 11–18, Jun. 2010.
[38] G. Schmid *et al.*, "Fabrication of 28nm pitch Si fins with DSA lithography," *Proc. SPIE*, vol. 8680, pp. 86801F-1-12, Mar. 2013.

Michael Wong received the B.Sc. degree in computer engineering from the University of Alberta, Edmonton, AB, Canada, in 2013, where he is currently pursuing the Ph.D. degree in electrical engineering.

His current research interests include the modeling and simulation of nanoscale devices, including FinFETs and 2-D FETs.

Kyle D. Holland (M'16) received the B.Sc. degree in engineering physics (nanoengineering option) from the University of Alberta, Edmonton, AB, Canada, in 2009, where he is currently pursuing the Ph.D. degree in electrical engineering.

His current research interests include the quantum simulation of carbon-based nanoelectronics, with a focus on modeling the high-frequency performance of graphene devices.

Sam Anderson is currently pursuing the B.Sc. degree in engineering physics (nanoengineering option) with the University of Alberta, Edmonton, AB, Canada.

He is involved in the technological and environmental adaptations that will impact human life in the 21st century. His current research interests include the use of novel materials in solar cell applications.

Shahriar Rizwan received the B.Sc. degree in electrical and electronic engineering from the Bangladesh University of Engineering and Technology, Dhaka, Bangladesh, in 2012. He is currently pursuing the Ph.D. degree in electrical engineering with the University of Alberta, Edmonton, AB, Canada.

He was a Software Engineer with the Samsung Research and Development Institute Bangladesh, Dhaka, from 2012 to 2014.

Zhi Cheng (Jason) Yuan received the B.Sc. degree in engineering physics (nanoengineering option) from the University of Alberta, Edmonton, AB, Canada, in 2014, where he is currently pursuing the Ph.D. degree in electrical engineering.

His current research interests include the simulation of high-speed integrated circuits, with a focus on the modeling of ferroelectric negative-capacitance FETs.

Terence B. Hook received the B.Sc. degree in electrical engineering from Brown University, Providence, RI, USA, in 1980, and the Ph.D. degree in electrical engineering from Yale University, New Haven, CT, USA, in 1986.

Since 1980, he has been with IBM Corporation, Essex Junction, VT, USA, where he has been involved in technology development and research in Essex Junction, VT, USA, East Fishkill, NY, USA, and Albany, NY, USA.

Diego Kienle received the Ph.D. degree in theoretical physics from the Research Center Juelich, Jülich, Germany, and University Saarland, Saarbrücken, Germany.

He is currently with the Institute of Theoretical Physics, University Bayreuth, Bayreuth, Germany. His current research interests include the theory and simulation of quantum kinetic transport in nanoscale materials and devices.

Prasad S. Gudem (M'96-SM'15) received the B.Tech. degree in electrical engineering from IIT Madras, Chennai, India, in 1988, and the Ph.D. degree in electrical engineering from the University of Waterloo, Waterloo, ON, Canada, in 1996.

He is currently a Vice-President of Engineering with the Analog/RF Integrated Circuit Design Group, Qualcomm Technologies Inc., San Diego, CA, USA.

Mani Vaidyanathan (M'99) received the Ph.D. degree in electrical engineering from The University of British Columbia, Vancouver, BC, Canada.

He is currently an Associate Professor with the Department of Electrical and Computer Engineering, University of Alberta, Edmonton, AB, Canada. His current research interests include the modeling, simulation, and understanding of electronic devices for future electronics, with a focus on the radio-frequency performance of FinFETs and 2-D materials.